ISSN 2319-5991 www.ijerst.com
© 2026 IJERST. All Rights Reserved
Peer Reviewed, Referred & Indexed Journal

Research Paper

Analysis of ANN-Based Control for Grid-Connected Single-Phase Rooftop PV Systems with Enhanced Power Quality

Dr. S. Jagadish Kumar[1], B. Soumya[2]

[1]Associate Professor, Department of Electrical and Electronics Engineering, JNTUH University College of Engineering (Autonomous) Jagtial, Telangana, India.

[2] PG, M. Tech (Electrical Power Systems), Department of Electrical and Electronics Engineering, JNTUH University College of Engineering (Autonomous) Jagtial, Telangana, India.

***Abstract:** A large portion of grid-connected, low-voltage PV systems installed on residential roofs employ inverter management algorithms that aren't adaptable enough to deal with nonlinear operating conditions, grid outages, and rapid changes in solar radiation. Using an ANN-based control technique, it deals with a grid-connected, single-phase rooftop photovoltaic (PV) system that improves power quality. Instead of a conventional PI controller, the proposed approach uses an ANN controller to regulate the dc-link voltage and grid-injected current. A controller trained to deal with nonlinearities and system dynamics may improve tracking accuracy, transient responsiveness, and reliability over a variety of grid and weather conditions. The grid-connected photovoltaic (PV) system is developed and validated in MATLAB/Simulink. An LC-L filter is incorporated at the inverter output to effectively attenuate high-frequency switching harmonics, minimize total harmonic distortion (THD) in the injected grid current, and ensure compliance with IEEE-519 power quality standards while maintaining stable and reliable grid operation.*

***Keywords:** Photovoltaic (PV), ANN controller, Power Quality.*

I.INTRODUCTION

Integrating small-scale photovoltaic systems (PV) into distributed generation (DG) networks has become more important due to the fast growth of renewable energy sources [1]. Reliability, efficiency, and reduced operational costs are three primary goals of these systems [2]. Several converter topologies have been studied by scientists that want to increase power density while minimizing system cost [2, 3]. However, power density and system reliability are both negatively impacted by a high number of power conversion processes. For increased efficiency and reliability, grid-connected photovoltaic (GCPV) systems often use single-stage power converters.

However, single-stage GCPV systems may have instability due to the dc-link voltage dynamics changing too quickly, notwithstanding these benefits. It is becoming more difficult to keep systems stable during grid disruptions such voltage sag, load changes, and irradiance fluctuations due to the growing number of PV-based DG systems. Consequently, in order to keep the system stable, a controller with a quick dynamic reaction is required. Response times, which are usually less than 0.1 s for the dc-link voltage controller and less than 0.01 s for the current controller, are the main metrics used to evaluate the dynamic performance of these systems [4, 5]. This has led to several proposals for cutting-edge control systems that aim to improve system efficiency. To enhance dynamic performance and voltage regulation, it is common practice to include an all-pass filter into the current loop and use a strong outer-loop voltage controller[6]. The operation of single-stage GCPV systems is dependent on the simultaneous execution of dc-link voltage control, PV source power optimization, and grid current reference generation. System stability and excellent power quality remain key challenges, nevertheless. Adding more poles to the system using an LC-L filter can potentially cause instability and resonance problems [8]. Active damping current controllers are a popular method for addressing this issue [9]. Consequently, disruptions on both the grid and PV sides need controllers with strong capabilities.

In order to improve system performance and decrease disturbance effects, intelligent and nonlinear control strategies have been proposed recently [10]-[14]. With these controllers in place, system dynamics are enhanced, and stability margins are widened. However, feedback linearization and other nonlinear methods utterly bomb when testing power quality [12], [13]. There have been several advanced controllers suggested for managing the current and dc-link voltage, including μ-synthesis and H∞ controllers [14]. Complexity, switching frequency, and dc-link voltage ripple are some of the drawbacks of these controllers, however they are robust to changes in grid impedance and time delay effects. For better system performance and disturbance rejection, other control approaches such adaptive gain observers and active disturbance rejection controllers (ADRC) have also been studied [15], [16]. These controllers increase system complexity and may introduce steady-state errors and switching frequency variations. In single-phase grid-connected PV systems, dc-link voltage oscillations, grid disturbances, and PV power intermittency degrade power quality and increase harmonic distortion, necessitating robust control with fast transient response.

Another reason the system can shut down is if there is a large voltage spike across the dc-link, which might damage the inverter switches or the dc-link capacitor [17]. Adaptive PI and nonlinear PI (NPI) controllers may be used to alter the dc-link voltage and reduce harmonics in single-phase systems [18]-[20]. These solutions rely on gain recalculation, complicated computing, or predictive modelling, all of which may increase efficiency but also increase the difficulty of implementing them.

There have been many methods investigated for reducing the impact of double-frequency ripple on reference current output. Some examples of such methods include notch filters, active decoupling circuits, and moving average filters (MAF) [21, 22]. Potential threats to system stability include changes in system characteristics and load interruptions, which may disrupt the management of dc-link voltage and grid current quality [25], [26]. In response to these issues, it suggests a more effective control method for a single-phase, grid-connected PV system. To make the system more responsive and adaptable, an intelligent controller built on ANNs is suggested to replace the traditional controller. Incorporating an ANN controller into your system has several benefits, including improved dc-link voltage management, enhanced disturbance rejection, and lower grid current harmonics. Also, it might be able to pick up on system nonlinearities. The LC-L filter does double duty by enhancing power quality and decreasing switching harmonics.

II. SYSTEM CONFIGURATION

An LC-L filter integrated single-phase grid-connected photovoltaic (GCPV) system is shown schematically in Fig 1. The design of the system has an emphasis on producing stable and high-quality electricity via effective conversion of solar energy into electrical power and injection into the utility grid. The one-phase utility grid, a PV array, a dc-link capacitor, a VSI, an LC-L filter, and the setup are the necessary components.

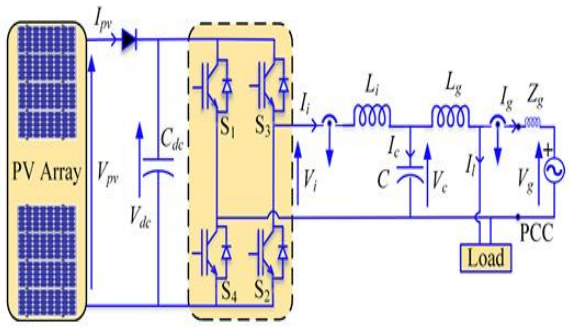

Fig. 1. Single-stage PV integrated grid-connected inverter system with an LCL filter.

The photovoltaic (PV) array is a crucial component of any power plant because it converts heat and sunlight into direct current (DC) energy. A dc-link capacitor (C_{dc}) is required to connect the PV array to the VSI due to the PV array's output voltage fluctuations. A capacitor that can absorb energy and decrease voltage waves is necessary to keep the dc-link voltage constant, particularly in dynamic settings. The DC-link capacitor maintains a stable DC voltage for reliable inverter operation in a single-stage PV system. The inverter converts the PV array's DC power into AC power and synchronizes it with the grid using appropriate control and modulation techniques. An LC-L filter is used to remove switching harmonics, improve power quality, reduce THD, and ensure that the injected grid current is sinusoidal and in phase with the grid voltage, achieving unity power factor.

A state-space model accurately represents the dynamic behavior of a single-stage grid-connected PV (GCPV) system by describing the interactions among the PV array, inverter, DC-link capacitor, filter, and grid. It supports controller design, performance analysis, and system stability evaluation. The LC-L filter improves power quality by reducing harmonics, while the DC-link capacitor maintains a stable voltage, enabling efficient and reliable grid-connected solar power generation.

$$L_i \frac{di_i}{dt} = s_u v_i - v_c - r_i i_i \qquad C \frac{dv_c}{dt} = i_i - i_g$$

$$L_g \frac{di_g}{dt} = v_c - v_g - r_g i_g \qquad C_{dc} \frac{dv_{dc}}{dt} = i_{pv} - s_u i_i \tag{1}$$

$$\frac{d}{dt}\begin{bmatrix} i_g \\ i_i \\ v_c \\ v_{dc} \end{bmatrix} = \begin{bmatrix} -\tau_g^{-1} & 0 & L_g^{-1} & 0 \\ 0 & -\tau_i^{-1} & -L_i^{-1} & s_u L_i^{-1} \\ -C^{-1} & C^{-1} & 0 & 0 \\ 0 & -s_u C_{dc}^{-1} & 0 & 0 \end{bmatrix} \begin{bmatrix} i_g \\ i_i \\ v_c \\ v_{dc} \end{bmatrix} + \begin{bmatrix} -L_g^{-1} v_g \\ 0 \\ 0 \\ r_{pv}^{-1} C_{dc}^{-1} v_{pv} \end{bmatrix} \tag{2}$$

The inverter's time constant is $\tau_i(= L_i/r_i)$ while the grid-side inductor's time constant is $\tau_g(= L_g/r_g)$. $V_i = s_u$ is the inverter's output voltage, hence. The four inverter switches {1, 2, 3, 4} and their switching function are represented by V_{dc} and s_u, respectively, they manage the inverter system. Consider the steady-state switching function and the perturbation deviation of u in the set by expressing it as $s_u = S_u + \Delta s_u$. The system model may be described using two methods: the grid side's current control and the PV side's dc-link voltage control. The following formula may be used to define grid control and PV side control in the same vein:

$$x_1 = i_i - i_{iref} \qquad x_3 = v_c - v_{cref}$$

$$x_2 = i_g - i_{gref} \qquad x_4 = v_{dc} - v_{dcref} \qquad (3)$$

III. DC-LINK CONTROL AND CURRENT QUALITY IMPROVEMENT

The controller for a single-stage, single-phase GCPV system is shown in Fig.2. An incremental conductance-based MPP tracking (MPPT) technique is used to effectively run a solar array at its maximum power point (MPP), as seen in Fig. 3. The MPPT control directs the maximum PV power to the grid while maintaining a constant dc-link voltage (V^*_{dc}) [23], [27]. Additionally, a maximum power feedforward loop described by (6) is used to enhance MPP tracking, and the dc-link voltage controls the amount of grid current. Even in the face of voltage changes, the feedforward is essential for controlling the maximum power from PV to the grid. It is suggested to combine NPI and MAF control to enhance dynamic responsiveness and lessen the impact of double line frequency. One way to characterize the maximum reference grid current is as

$$I_m = I_{ff} - I_{loss} \qquad (4)$$

$$I_{ff} = \frac{\sqrt{2}Ppv}{Vgm} \qquad (5)$$

The MPPT algorithm determines the PV output power, which is used to generate the reference grid current. The outer loop controller regulates the DC-link voltage and compensates for power losses, while the Lyapunov-based inner loop controller ensures fast dynamic response, zero steady-state error, and stable current tracking. A capacitor voltage loop provides resonance damping for the LC-L filter, improving system stability and grid power quality.

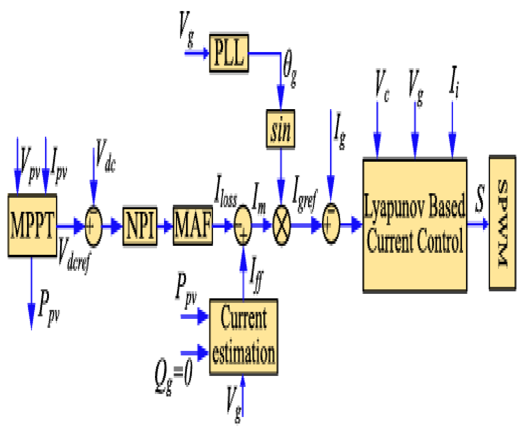

Fig. 2. Proposed control structure for the single-phase single-stage GCPV system.

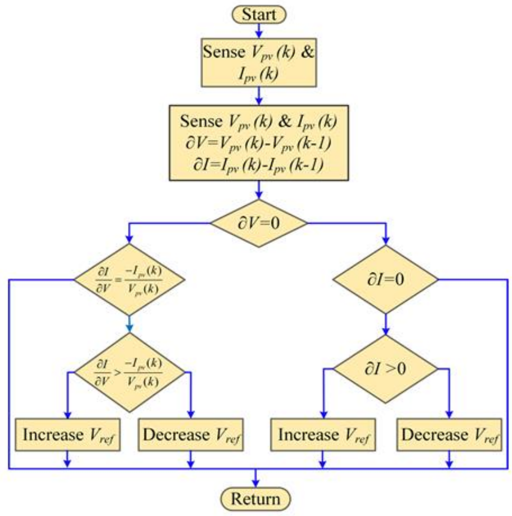

Fig. 3. The incremental conductance MPPT algorithm's flowchart.

While traditional systems that use an outer voltage control loop, grid-connected PV (GCPV) systems use an inner current control loop for better dynamic performance. The DC-link voltage is treated as a state variable and serves as the input to the current controller. By using the control input (u) and output (y), a plant model can be developed for effective DC-link voltage regulation.

$$\dot{y}(t) = d_i + u \qquad (6)$$

where d_i is the input disturbance to the system [28]. A possible error-based representation of the target dc-link controller output is as

$$\dot{x_4} = - d_i - u \qquad (7)$$

Given the existence of disturbance di, the closed-loop system's control logic must ensure that, as t approaches infinity, $x_4(t) \rightarrow 0$, so that the reference may be fully followed. Therefore, a regular PI controller might be used as

$$u_c(t) = k_p x_4 + k_i \int x_4 \, dt \qquad (8)$$

where integral benefits are denoted by k_i and proportional gains are represented by k_p. Bode diagrams and pole placement optimization are two popular control design strategies for changing the voltage control loop [17]. The NPI-based DC-link voltage controller provides a fast dynamic response with minimal overshoot. It regulates the DC-link voltage by comparing the actual and reference voltages obtained from the MPPT algorithm. The nonlinear gain function fal(x_4) improves disturbance rejection, enhances stability, and reduces steady-state error by applying higher gain for small errors and lower gain for large errors.

$$fal(x_4)=\begin{cases} |x_4|^m \, sgn(x_4), & |x_4| > \delta p \\ x_4 / \delta_p^{(1-m)}, & |x_4| \le \delta p \end{cases}, \delta p > 0 \qquad (9)$$

The nonlinear gain function fal(x_4) uses the signum function and parameter δ_p to limit controller gain and improve stability. Selecting $0 < m < 1$ provides faster convergence, better disturbance rejection, and reduced steady-state error. Compared to integral control, fal(x_4) eliminates phase delay, offering a wider stability margin and near zero steady-state error. The controller becomes less noise-sensitive, nevertheless, thanks to it [28].

The outer-loop NPI controller regulates the DC-link voltage by adaptively adjusting the gain, improving dynamic response and reducing voltage oscillations. A Moving Average Filter (MAF) suppresses DC noise and low-frequency ripple, enhancing grid current quality and lowering THD. The Lyapunov-based inner current controller ensures global stability, accurate current tracking, and unity power factor, while the PR controller improves steady-state accuracy. Active damping using capacitor voltage feedback suppresses LCL filter resonance and further enhances harmonic performance.

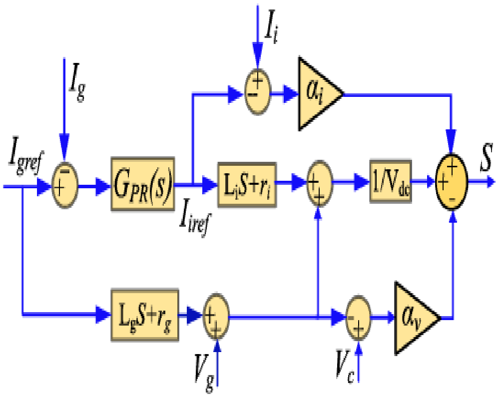

Fig. 4. Lyapunov-based inner loop control structure.

The Lyapunov-based inner current controller ensures stable operation, accurate current tracking, sinusoidal grid current, and unity power factor. A PR controller eliminates steady-state tracking errors, while capacitor voltage feedback provides active damping to suppress LCL filter resonance. The NPI outer-loop controller improves dynamic response with adaptive gains, minimizes overshoot, and enhances disturbance rejection. Proper DC-link capacitor selection reduces voltage ripple and improves overall system stability, efficiency, and harmonic performance.

$$s_u = S_u + \alpha_i \left(i_{iref}\, x_4 - V_{dcref} x_1 \right) \qquad (10)$$

Where,

$$S_u = \frac{1}{V_{dcref}} \left(L_i \frac{V i_{iref}}{dt} + r_i\, i_{iref} + v_{cref} \right) \qquad (11)$$

The control strategy starts with a PI controller to obtain initial gains, which are used as reference values for the NPI controller. The NPI controller adaptively adjusts its gain to improve dynamic response, reduce overshoot, and enhance steady-state accuracy. Thresholds δ_p and δ_i minimize chattering and prevent integrator windup. Combined with the Lyapunov-based inner current controller and an optimally selected DC-link capacitor, the system achieves faster response, lower harmonics, improved stability, and reliable operation under varying conditions.

IV. ANN CONTROLLER

In this, the traditional PI controller is beaten by an ANN-based controller when it comes to controlling voltage and current. In contrast to PI control, ANN can better capture nonlinear dynamics by training using input-output data from systems with various loads and grid circumstances. As a consequence, there is a better chance of two batteries sharing power more efficiently during transients, and control precision, dynamic responsiveness, power factor adjustment, and reduction of total harmonic distortion (THD) are all enhanced.

The below fig.5 shows a multilayer feedforward artificial neural network (ANN) with backpropagation is built. Levenberg-Marquardt outperforms gradient descent and Gauss-Newton as a training algorithm in terms of convergence speed and learning capacity. An input layer, a hidden layer with ten neurons, and an output layer make up an artificial neural network's structure. Inputs are the d-q frame-appearing error and change in error signals, while outputs are the abc component-represented control signals. In order to keep the system running smoothly and accurately, the controller must minimize the MSE, or mean square error, between the reference and real values.

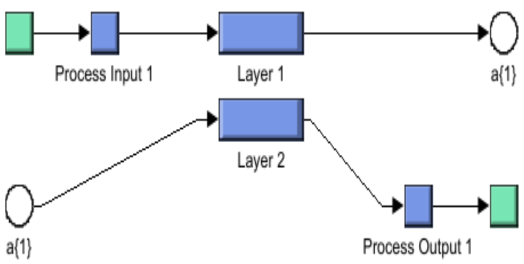

Fig.5. Typical Structure of ANN control

V. SIMULATION RESULTS

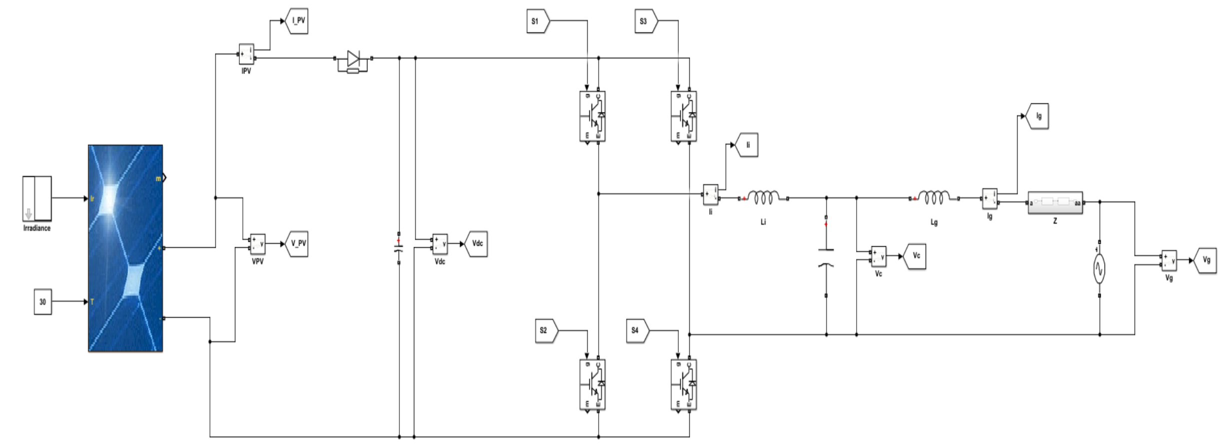

Fig. 6. MATLAB/SIMULINK was used to simulate the proposed grid-connected inverter system for single-stage photovoltaics with an LCL filter.

The above Fig.6 shows a MATLAB/Simulink model of the proposed single-stage grid-connected PV system. The PV array generates DC power based on irradiance and temperature, which is stabilized by a DC-link capacitor. A single-phase full-bridge inverter converts the DC power into AC using PWM control signals. The inverter output passes through an LCL filter to reduce switching harmonics before supplying clean power to the utility grid. Voltage and current measurement blocks provide the feedback required for system control, synchronization, and performance analysis.

A) RESULTS WITH PI CONTROLLER

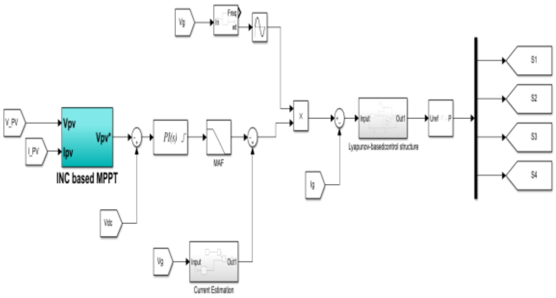

Fig.7. Control system of PI Controller.

The above Fig.7 represents the control structure of the grid-connected PV system. The INC-based MPPT generates the reference PV voltage, while the PI controller and moving average filter produce the reference grid current. A Lyapunov-based current controller ensures accurate current tracking, and the PWM gating signals (S_1–S_4) synchronize the inverter with the grid.

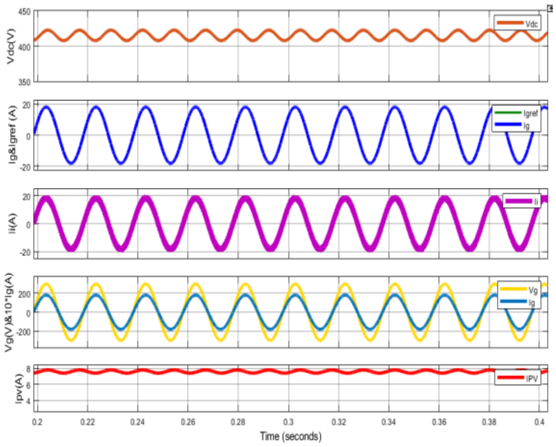

Fig.8. Simulation results showing performance of the PI controller in steady state while transferring rated power into the grid at UPF.

The above Fig.8 shows the steady-state performance of the grid-connected PV system. The DC-link voltage remains stable, the grid and inverter currents are sinusoidal with accurate current tracking, and the grid voltage and current are in phase, confirming unity power factor. The PV current remains constant, indicating successful MPPT and efficient power extraction.

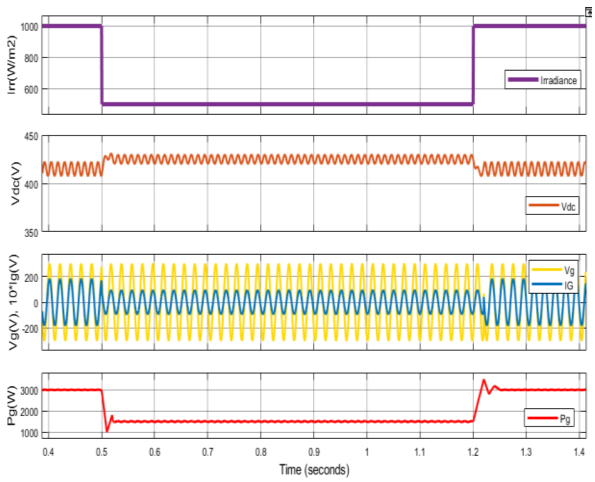

Fig.9. Simulation results showing dynamic performance of GCPV system with PV-side disturbances.

The above Fig.9 shows a irradiance waveform changes in solar intensity. During irradiance variations, the DC-link voltage remains stable with small fluctuations, while the grid voltage stays sinusoidal. The grid current and active power vary according to the available solar power, confirming effective MPPT, smooth power injection, and unity power factor operation.

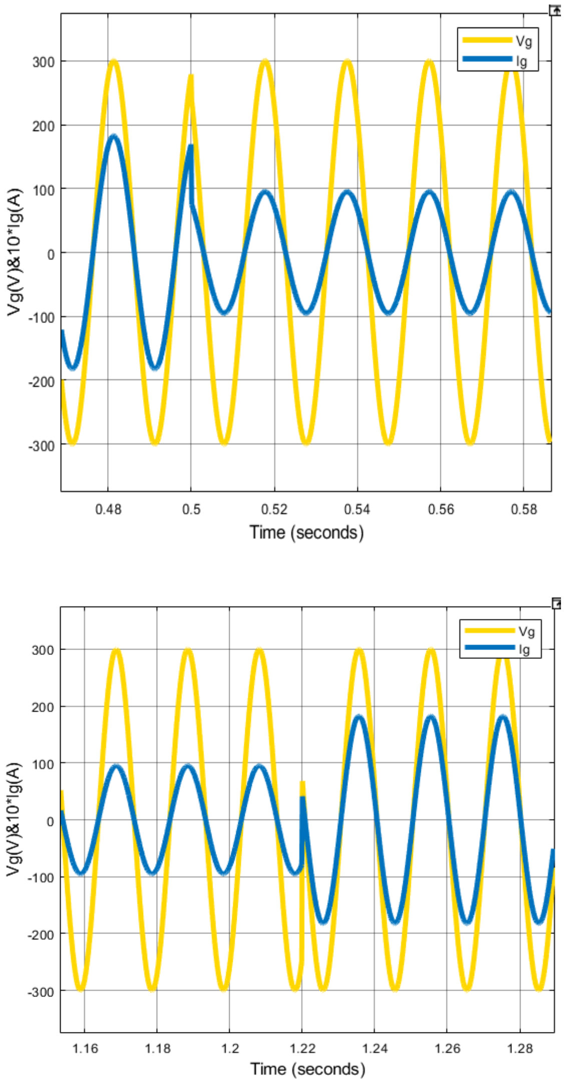

Fig.10. Zoomed-in view showing the grid current and grid voltage under step change in irradiance.

The above Fig.10 shows the zoomed-in grid voltage (V_g) and grid current (I_g) during irradiance changes. The grid voltage remains stable and sinusoidal, while the grid current changes its amplitude according to the available solar power. The current remains in phase with the grid voltage, confirming unity power factor, fast dynamic response, and effective current control.

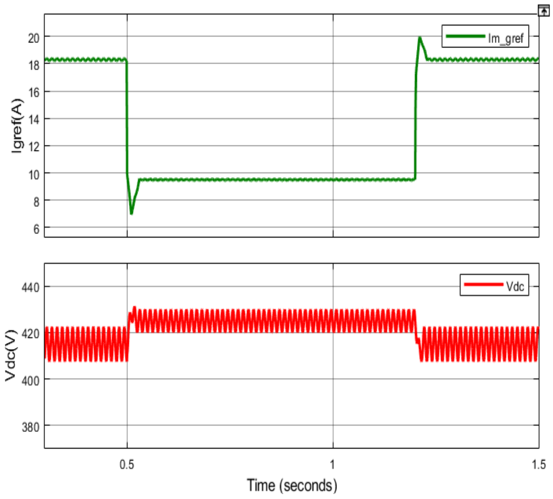

Fig.11. Zoomed-in view of PI controller performance, showing reference grid current and dc-link voltage.

The above Fig.11 shows the dynamic response of the grid current reference (I_{gref}) and DC-link voltage (V_{dc}) during a step change. The grid current quickly tracks the reference with minimal overshoot, while the DC-link voltage experiences only a small transient and rapidly returns to its reference value. These results demonstrate fast current tracking, stable DC-link voltage regulation, and excellent dynamic performance.

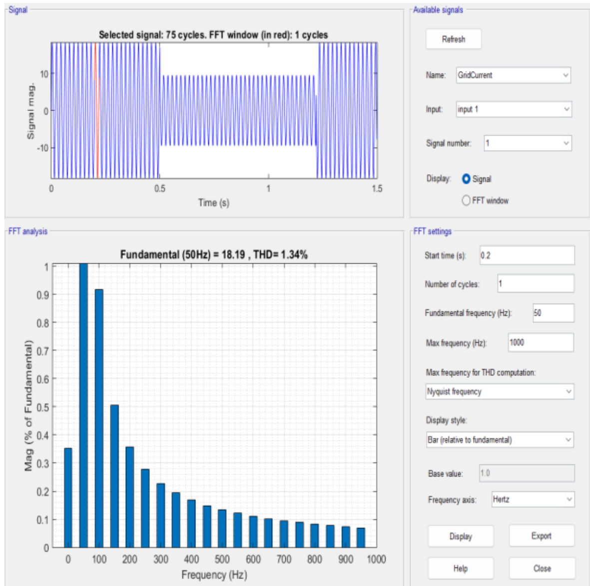

Fig.12. THD% of Grid current under steady state.

The above Fig.12 shows a stronger 50 Hz fundamental component and a low THD of 1.34%, confirming improved harmonic performance and effective reduction of current distortion.

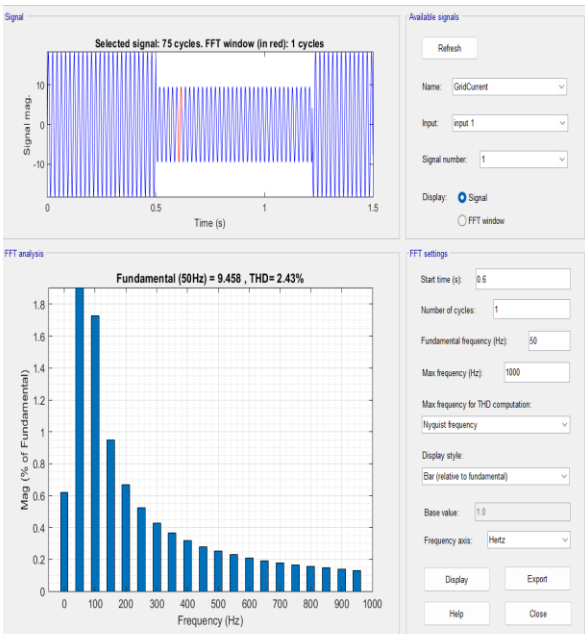

Fig.13. THD% of Grid Current Under Dynamic State.

The above Fig.13 shows a dominant 50 Hz fundamental component with low harmonic content and a THD of 2.43%, confirming high-quality grid current injection and compliance with power quality standards.

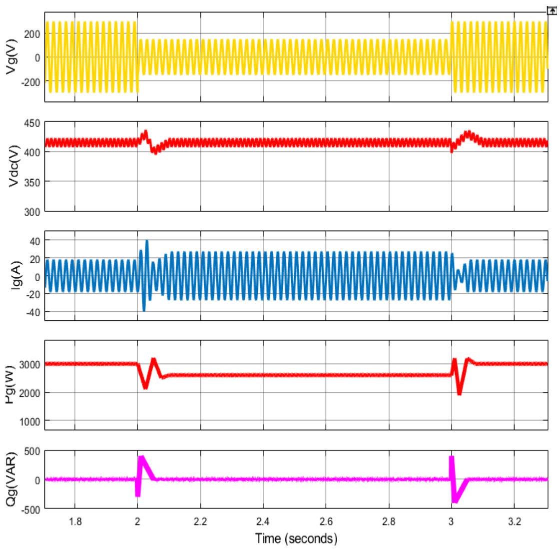

Fig.14. Simulation results showing the performance of the controller under grid-side disturbances, considering 50% voltage sag in the grid voltage.

The above Fig.14 shows the dynamic performance of the grid-connected PV system during step changes. The grid voltage remains stable and sinusoidal, the DC-link voltage quickly returns to its reference value, and the grid current adjusts smoothly with power variations. The active power follows the available PV power, while the reactive power remains close to zero, confirming fast response, stable operation, and unity power factor.

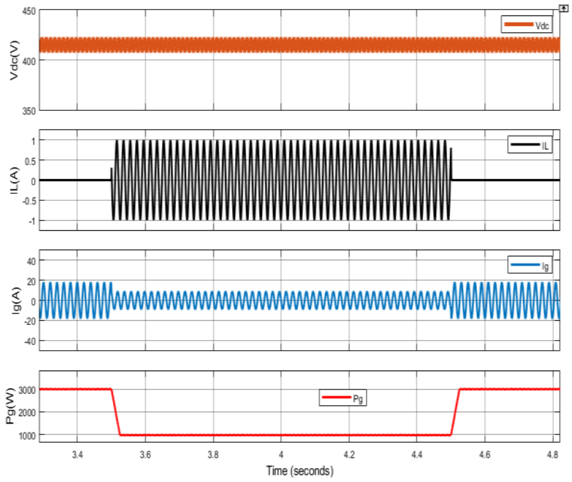

Fig.15. Performance of the controller under sudden connection and disconnection of the local load at PCC.

The above Fig.15 shows a DC-link voltage remains stable with minimal ripple, indicating effective voltage regulation during load changes. The load and grid currents remain sinusoidal, while the grid power varies according to the load with fast settling and minimal oscillations, confirming stable operation, reliable power transfer, and good grid synchronization.

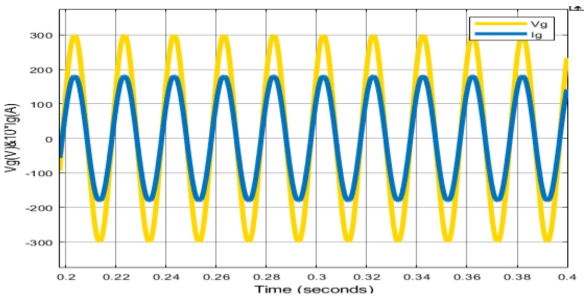

(a)

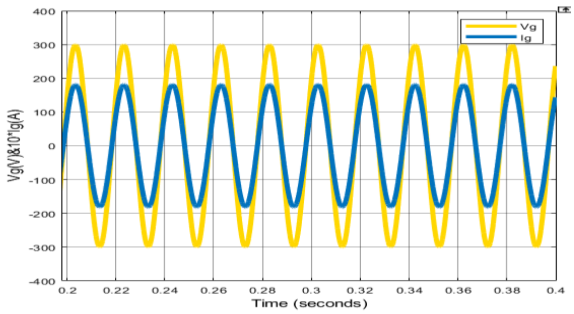

(b)

Fig. 16. Simulation results showing the robustness of the controller under parametric uncertainties. (a) Considering 20% change in filter parameter and (b) with high grid impedance (Z_g = 0.1, 4.25 mH).

The above Fig.16 shows the controller's robustness under varying operating conditions. During sudden load changes, the grid power responds quickly and settles smoothly. Even with filter parameter variations and high grid impedance, the grid voltage and current remain sinusoidal and synchronized, confirming stable operation, good power quality, and strong controller performance.

B) RESULTS WITH ANN CONTROLLER

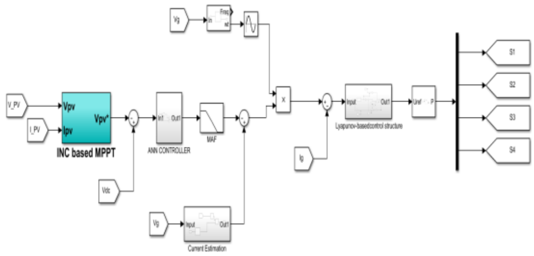

Fig.17. Control system of ANN Controller.

The above Fig.17 shows control structure of the grid-connected PV system using an ANN and Lyapunov-based controller. The INC-based MPPT generates the reference voltage, while the ANN controller regulates the DC-link voltage. A Moving Average Filter (MAF) smooths the signal, and the Lyapunov controller ensures accurate grid current tracking. Finally, PWM signals (S_1–S_4) control the inverter, achieving maximum power extraction, stable operation, and improved power quality.

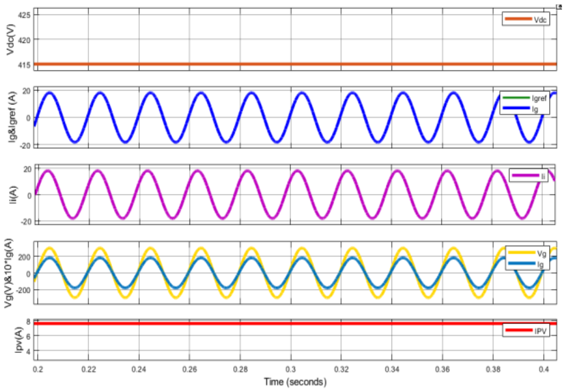

Fig.18. Simulation results showing performance of the ANN controller in steady state while transferring rated power into the grid at UPF.

The above Fig.18 shows the steady-state performance of the grid-connected PV system. The DC-link voltage remains stable at its reference value, the grid current accurately tracks its reference, and the load current is sinusoidal. The grid voltage and current are in phase, confirming unity power factor, while the constant PV current indicates stable power generation and efficient system operation.

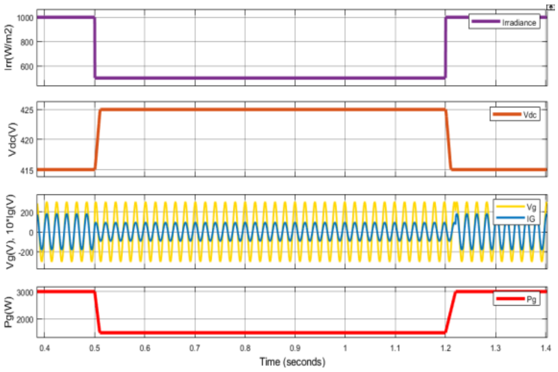

Fig.19. Simulation results showing dynamic performance of GCPV system with PV-side disturbances.

The above Fig.19 shows the performance of the grid-connected PV system under varying solar irradiance. The DC-link voltage remains stable, while the grid voltage and current stay sinusoidal. The grid current and active power vary according to irradiance, demonstrating stable operation, effective control, and good power quality under dynamic conditions.

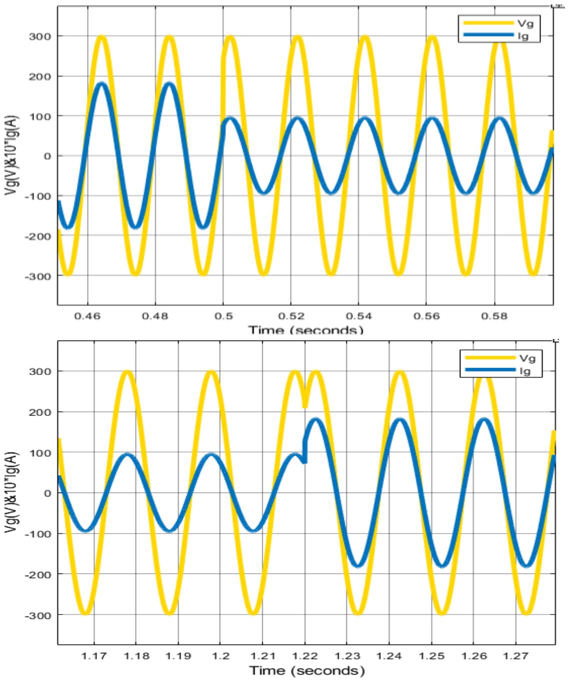

Fig.20. Zoomed-in view showing the grid current and grid voltage under step change in irradiance.

The above Fig.20 shows the grid voltage (V_g) and grid current (I_g) waveforms. The grid voltage remains sinusoidal, while the grid current quickly settles after a brief transient and stays in phase with the voltage. This confirms fast controller response, good grid synchronization, unity power factor, and high-power quality.

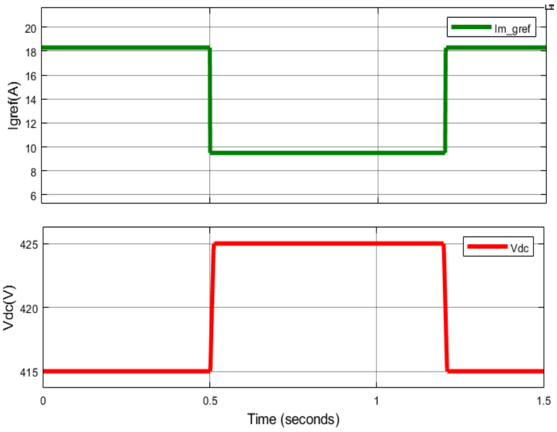

Fig.21. Zoomed-in view of ANN controller performance, showing reference grid current and dc-link voltage.

The above Fig.21 shows the variation of the reference grid current (I_{gref}) and DC-link voltage (V_{dc}). The controller quickly adjusts the current during operating changes, while the DC-link voltage experiences only small fluctuations and remains stable, demonstrating effective current control and voltage regulation.

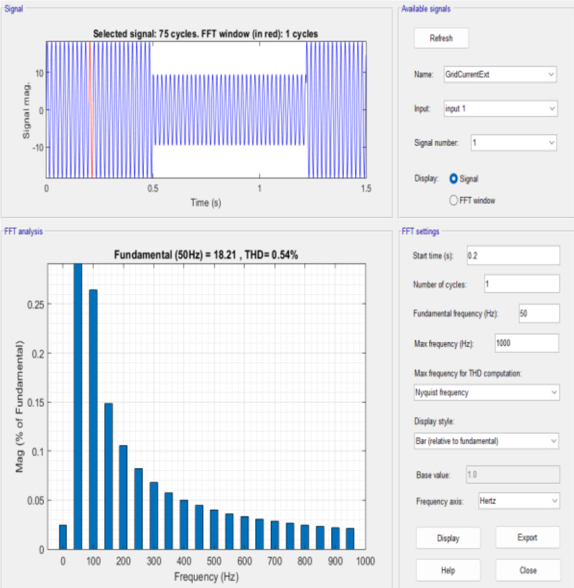

Fig.22. THD% of Grid current under steady state.

The FFT analysis shows a dominant 50 Hz fundamental component with a very low THD of 0.54%, indicating negligible harmonic distortion, excellent power quality, and stable grid current operation.

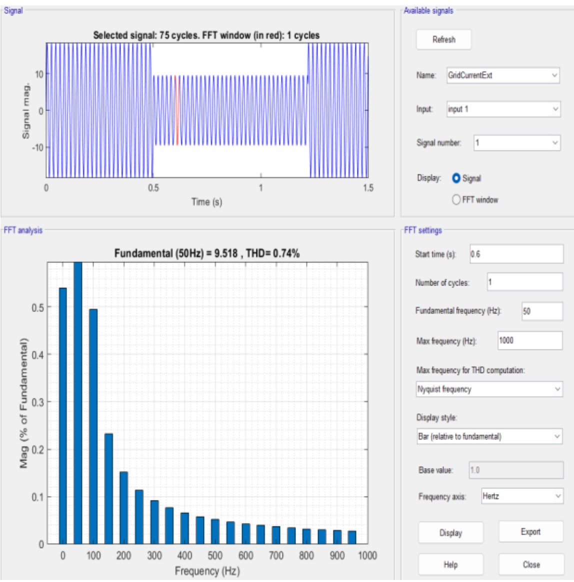

Fig. 23. THD% of Grid Current Under Dynamic State.

The above Fig.23 shows the FFT analysis of the grid current under dynamic conditions. The spectrum has a dominant 50 Hz fundamental component with a low THD of 0.74%, indicating minimal harmonic distortion and good power quality even during dynamic operation.

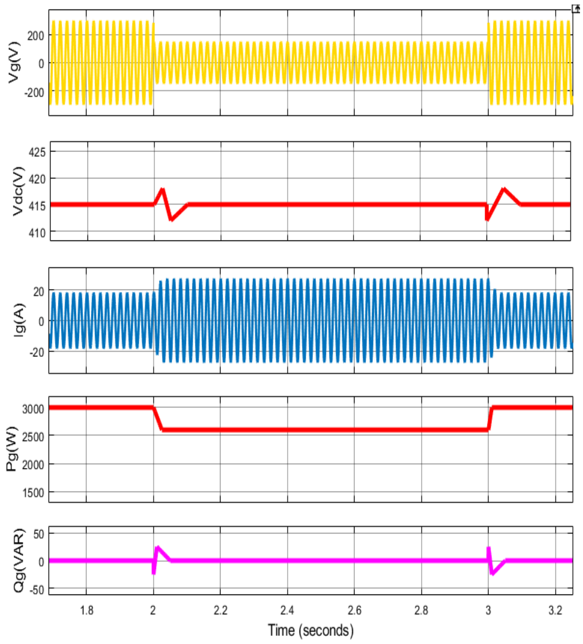

Fig.24. Simulation results showing the performance of the controller under grid-side disturbances, considering 50% voltage sag in the grid voltage.

The above Fig.24 shows the dynamic performance of the grid-connected PV system. The grid voltage remains sinusoidal, the DC-link voltage stays stable with minor fluctuations, and the grid current adjusts smoothly with power changes. The active power varies according to operating conditions, while the reactive power remains close to zero, confirming effective control, stable operation, and good power quality.

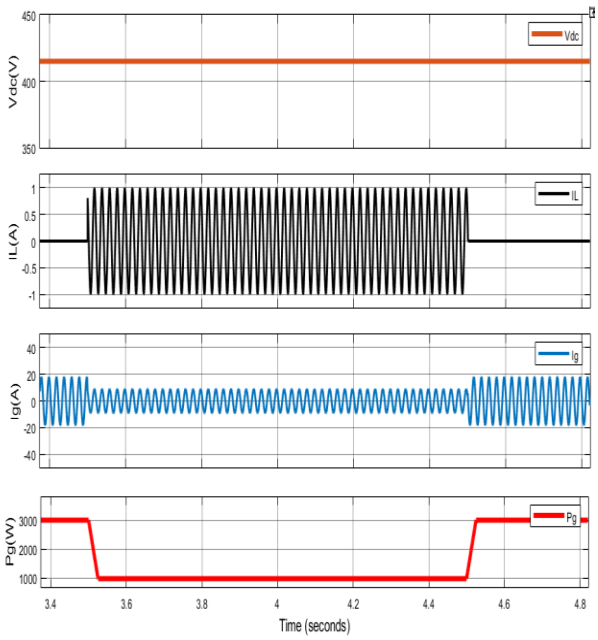

Fig.25. Performance of the controller under sudden connection and disconnection of the local load at PCC.

The above Fig.25 shows the system performance during load variation. The DC-link voltage remains stable, while the grid current adjusts its amplitude according to load demand and stays sinusoidal. The active power changes with the load, demonstrating fast response, stable operation, and good power quality.

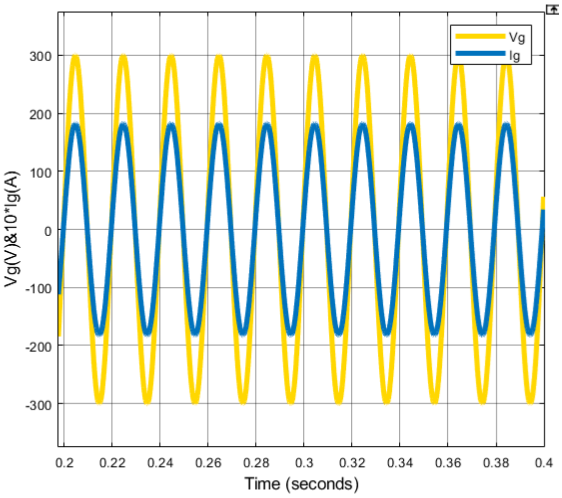

(a)

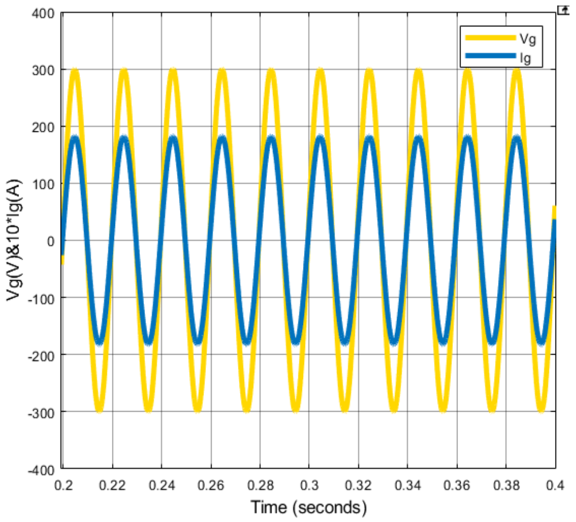

(b)

Fig.26. Simulation results showing the robustness of the controller under parametric uncertainties. (a) Considering 20% change in filter parameter and (b) with high grid impedance (Z_g = 0.1 , 4.25 mH).

The above Fig.26 shows the grid voltage (V_g) and grid current (I_g) waveforms. Both are sinusoidal and in phase, confirming unity power factor, proper grid synchronization, low harmonic distortion, and high-power quality.

COMPARSION TABLE

S. No	Performance Parameter	PI Controller	ANN Controller
1	Control System Structure	PI-based control system	ANN-based intelligent control system
2	Steady-State Performance	PV grid-connected inverter delivering rated power at UPF	Improved steady-state performance with ANN control
3	Dynamic Performance with PV Disturbances	System response under PV irradiance variation	Faster dynamic response using ANN controller
4	Grid Current and Grid Voltage (Zoomed View)	Grid current tracking under irradiance step change	Improved current tracking accuracy
5	DC-Link Voltage and Reference Grid Current	DC-link voltage regulation using PI control	Enhanced DC-link voltage stability with ANN
6	THD of Grid Current (Steady State)	1.34%	0.54%
7	THD of Grid Current (Dynamic Condition)	2.43%	0.74%
8	Grid Voltage Sag Performance	Controller performance during 50% grid voltage sag	Improved voltage sag compensation

CONCLUSION

It presents a control strategy for grid-connected single-phase rooftop photovoltaic (PV) systems to improve power quality and overall system performance. The developed approach is based on an improved Artificial Neural Network (ANN) controller. When it comes to managing grid-injected current and dc-link voltage, the suggested controller outperforms the existing PI-based control technique. System stability and unity power factor are not compromised as it adapts progressively to fluctuating grid disturbances and sun irradiation. When compared to the traditional PI controller, the ANN control approach achieves better results in the simulated system improved control of the dc-link voltage in the presence of transients such as changes in irradiance and load, accelerated dynamic response, and decreased total harmonic distortion (THD) in the grid current are all advantages of the improved controller. The capacity of the controller to maintain optimal operation increases the system's resistance to disturbances to the grid. Thus, the ANN control approach offers a reliable and efficient alternative to grid-connected rooftop PV systems. The developed control strategy demonstrates superior dynamic performance, enhanced voltage regulation, and reduced harmonic distortion, making it a reliable and efficient solution for grid-connected distributed generation systems with high renewable energy penetration.

REFERENCES

[1] R. Teodorescu, M. Liserre, and P. Rodríguez, Grid Converters for Photovoltaic and Wind Power Systems. Hoboken, NJ, USA: Wiley, 2011.

[2] F. Blaabjerg, R. Teodorescu, M. Liserre, and A. V. Timbus, "Overview of control and grid synchronization for distributed power generation systems," IEEE Trans. Ind. Electron., vol. 53, no. 5, pp. 1398–1409, Oct. 2006.

[3] J. M. Guerrero, J. C. Vasquez, J. Matas, L. G. De Vicuña, and M. Castilla, "Hierarchical control of droop-controlled AC and DC microgrids—A general approach toward standardization," IEEE Trans. Ind. Electron., vol. 58, no. 1, pp. 158–172, Jan. 2011.

[4] L. A. Zadeh, "Fuzzy sets," Information and Control, vol. 8, no. 3, pp. 338–353, 1965.

[5] S. Haykin, Neural Networks and Learning Machines, 3rd ed. Upper Saddle River, NJ, USA: Prentice Hall, 2009.

[6] M. Liserre, F. Blaabjerg, and S. Hansen, "Design and control of an LCL-filter-based three-phase active rectifier," IEEE Trans. Ind. Appl., vol. 41, no. 5, pp. 1281–1291, Sept./Oct. 2005.

[7] H. Patel and V. Agarwal, "MATLAB-based modeling to study the effects of partial shading on PV array characteristics," IEEE Trans. Energy Convers., vol. 23, no. 1, pp. 302–310, Mar. 2008.

[8] T. Esram and P. L. Chapman, "Comparison of photovoltaic array maximum power point tracking techniques," IEEE Trans. Energy Convers., vol. 22, no. 2, pp. 439–449, Jun. 2007.

[9] F. Blaabjerg, Z. Chen, and S. B. Kjaer, "Power electronics as efficient interface in dispersed power generation systems," IEEE Trans. Power Electron., vol. 19, no. 5, pp. 1184–1194, Sept. 2004.

[10] S. B. Kjaer, J. K. Pedersen, and F. Blaabjerg, "A review of single-phase grid-connected inverters for photovoltaic modules," IEEE Trans. Ind. Appl., vol. 41, no. 5, pp. 1292–1306, Sept./Oct. 2005.

[11] J. He and Y. W. Li, "An enhanced microgrid load demand sharing strategy," IEEE Trans. Power Electron., vol. 27, no. 9, pp. 3984–3995, Sept. 2012.

[12] J. Matas, M. Castilla, L. G. De Vicuña, J. Miret, and J. C. Vasquez, "Virtual impedance loop for droop-controlled single-phase parallel inverters using a second-order general-integrator scheme," IEEE Trans. Power Electron., vol. 25, no. 12, pp. 2993–3002, Dec. 2010.

[13] B. Singh, S. Singh, A. Chandra, and K. Al-Haddad, "Comprehensive study of single-phase AC–DC power factor corrected converters," IEEE Trans. Ind. Informat., vol. 7, no. 4, pp. 540–556, Nov. 2011.

[14] S. Kouro et al., "Recent advances and industrial applications of multilevel converters," IEEE Trans. Ind. Electron., vol. 57, no. 8, pp. 2553–2580, Aug. 2010.

[15] Y. Yang, F. Blaabjerg, and H. Wang, "Low-voltage ride-through of single-phase transformerless photovoltaic inverters," IEEE Trans. Ind. Appl., vol. 50, no. 3, pp. 1942–1952, May/Jun. 2014.

[16] H. Abu-Rub, M. Malinowski, and K. Al-Haddad, Power Electronics for Renewable Energy Systems, Transportation and Industrial Applications. Hoboken, NJ, USA: Wiley, 2014.

[17] S. Jain and V. Agarwal, "A single-stage grid-connected inverter topology for solar PV systems with maximum power point tracking," IEEE Trans. Power Electron., vol. 22, no. 5, pp. 1928–1940, Sept. 2007.

[18] R. Pena, J. C. Clare, and G. M. Asher, "Doubly fed induction generator using back-to-back PWM converters and its application to variable-speed wind-energy generation," IEE Proc. Electr. Power Appl., vol. 143, no. 3, pp. 231–241, May 1996.

[19] P. Rodriguez, A. Luna, R. Teodorescu, I. Etxeberria-Otadui, and F. Blaabjerg, "Advanced grid synchronization system for power converters under unbalanced and distorted operating conditions," IEEE Trans. Ind. Electron., vol. 58, no. 1, pp. 127–138, Jan. 2011.

[20] M. Castilla, J. Miret, J. Matas, L. G. De Vicuña, and J. M. Guerrero, "Control design guidelines for single-phase grid-connected photovoltaic inverters with LCL filter," IEEE Trans. Ind. Electron., vol. 56, no. 11, pp. 4498–4506, Nov. 2009.